2008 IEEE International Conference on
Robotics and Automation
Pasadena, CA, USA, May 19-23, 2008

Path Guidance Control for a Safer Large Scale Dissipative Haptic Display

B. Dellon[1] and Y. Matsuoka[2]

Abstract—**The properties of dissipative haptic displays allow larger workspaces that permit a whole body interaction useful for sports, rehabilitation, and large-scale object design applications. To that end we designed and constructed the Brake Actuated Manipulator (BAM) with $2m^3$ workspace. Dissipative devices are capable of simulating virtual objects through resistance analogous to active devices. However, the challenge remains for path guidance paradigms because neither impedance nor admittance control can be used to actively steer limb movements. Here we first define a new way to create and track a path during path guidance with a twinned vector field to allow bilateral motion. Using this new path definition three controllers, velocity ratio, force cancelling, and force mapping are compared with and without visual feedback. The results indicate that both force controllers provide better guidance over velocity control; the force mapping technique resulted in the smoothest limb trajectory. The presence of visual feedback was found to be a critical factor for path guidance using dissipative devices.**

I. Introduction

Robotic assistance for rehabilitation therapy and sports medicine is becoming more commonplace as technology evolves. Integration of robotic manipulation into current rehabilitation practices holds the promise of improving the quality of physical rehabilitation, increasing the efficiency of therapists and allowing more flexible/programmable rehabilitation environments. In particular neuro-rehabilitation for chronic stroke patients is of interest, because brain plasticity can be leveraged through novel visuo-motor tasks encouraging the neuro-motor system to change patterns [1]. Robotic neuro-rehabilitation is being investigated using several robotic platforms.

One study uses visual feedback distortion to combat learned non-use in stroke victims with a PHANTOM robot [2]. The MANUS manipulator [3] is used to investigate robot-aided neuro-rehabilitation, and PUMA 560 is used for the mirror image movement enabler (MIME) [4]. In all studies, groups treated with a robotic device performed equally or better than human therapy alone, and evinced robotic manipulation may have a bearing on brain recovery.

Unfortunately, throughout these studies the subjects were always either constrained to a small workspace (PHANTOM), restricted to planar movements in a limited area (MANUS), or placed at the mercy of dual PUMA 560's (MIME), which are capable of producing a maximum HIC (Head Injury Criterion) greater than 500 [5]; more than enough to cause injury or death. The root of these safety concerns, and hence functional restrictions, lies in the energetically active approach for actuation; namely the large effective inertia associated with most modern robotic arms. To alleviate this issue a *passive* haptic device may be used.

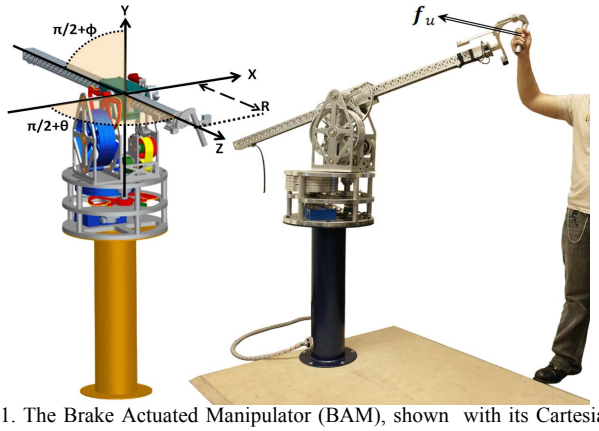

Fig 1. The Brake Actuated Manipulator (BAM), shown with its Cartesian and spherical coordinate system orientations. The BAM has $2m^3$ workspace sufficient for whole limb/body interactions.

There are three classes of passive haptic devices: hybrid steerable and dissipative. The main difference between these categories is the method of actuation. Hybrid devices, while not strictly passive, use a combination of motors and physical damping elements to increase control stability [6]. Steerable manipulators [7] use a continuously variable transmission, having fewer kinematic degrees of freedom than their workspace with the ability to reorient those DOFs. The main disadvantage here being the sizable side-slip traction devices like these exhibit. The third category of passive devices use brakes or clutches to dissipate or redirect energy. This is the type of passive device we focus on in this paper. Specifically we use a six DOF Brake Actuated Manipulator (BAM), with a sizable workspace of approximately two cubic meters (Fig.1) [8]. The large workspace allows us to train and quantify whole limb/body movements.

While dissipative devices such as the BAM can already perform similarly with conventional energetically actuated devices for object rendering, providing arbitrary path constraints is a greater technical challenge because of the inherent passivity constraint at each joint. Passive devices can only apply joint torques satisfying, $\tau_i \dot{q}_i \leq 0$; note that torque from a motor can satisfy either $\tau_i \dot{q}_i \leq 0$ or $\tau_i \dot{q}_i > 0$. Because there is no constraint for energetically actuated robots, either impedance or admittance control can be used to actively steer the user along a desired trajectory, while dissipative devices simply provide guidance to make a user stay close to a suggested path. We investigate this form of

[1]Mechanical Engineering, Carnegie Mellon University
[2]Computer Science and Engineering, University of Washington
This project was supported in part by NSF 0238204 and NIH R21HD47405

path following for dissipative devices, termed "path guidance."

One form of path guidance uses direct control with a serial two-link brake actuated device [9]. The brakes are controlled so the normal component of the resultant force is made to vanish using a passive force manipulability ellipsoid (FME) analysis. The main thrust of the work accounts for two distinct passive regions of the FME arising from the kinematics of passive serial devices. This technical issue is avoided with the BAM due to its orthogonal kinematics; allowing it to resist any force and maintain passivity at all joints [10]. This reduces the two distinct passive regions of the FME to one.

Three other controllers, the single DOF controller, velocity ratio, and optimal controllers have also been used for path guidance with the planar passive trajectory enhancing robot (PTER) [11-12], and are considered the state of the art in dissipative control. The single DOF controller is smoothly able to guide a user, assuming they are close to a single kinematic axis of the device. The velocity ratio controller defines the problem with a vector field, but often induces chatter in the actuator commands resulting in a bumpy feel and resulting paths. The optimal controller designed for PTER takes into account over-actuation created by mechanical coupling elements (clutch), but does not apply to our considerations because we lack any such coupling.

This paper focuses on the comparison between a modified velocity ratio controller, used on PTER [12], against our force cancelling and force mapping controllers. Each control technique is based on a bi-lateral vector field, allowing traversal both forwards and backwards. Experimentation is performed on multiple subjects to deduce variations between each control technique, with an eye towards the role of visual feedback in path guidance for a dissipative device.

II. Hardware Platform

A. Specifications & Sensing

The BAM (Fig. 1) is a six degree of freedom dissipative force feedback haptic robot, designed for rehabilitation and experimentation on the human musculoskeletal system through the simulation of virtual environments. It has been shown that a passively actuated robot must have orthogonal kinematics to control all the forces in the Cartesian space of the user [10]. The BAM's kinematics are spherical, not only to fulfill this requirement, but to achieve a low mass design.

The main spherical axes (pitch, yaw, extension) are controlled by magneto-rheological particle brakes, while the handle's three degrees of freedom remain un-actuated. The transmission stiffness varies between 2kNm/rad and 108kN/m respectively for the rotational and linear joints. The device is designed to resist a maximum force of 134N at full prismatic extension (1m). Full gravity compensation along the pitch axis is provided from an external passive spring mechanism and partial compensation is provided along the prismatic axis using the particle brakes in situ.

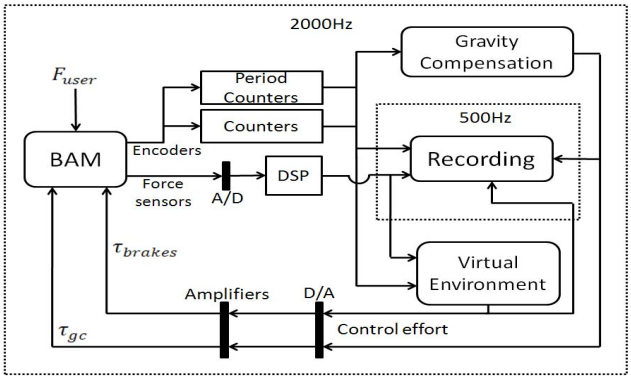

Fig 2. Schematic of data flow in and out of the BAM to the software controller, depicting inner recording loop running at a reduced frequency.

The BAM is controlled through custom multi-threaded software. The sensors and virtual environment physics/control are updated at a rate of 2kHz. Data recording, for post-processing, occurs concurrently at a lower frequency, ~500Hz; this helps reduce file size and increase program efficiency.

User forces are sensed with two pairs of ATI-Nano25 six axis force sensors situated at the handle's interface. The force signal is filtered with a recursive running sum filter with an invariant delay of 25ms. This delay in the control loop is acceptable when taking into account the limited bandwidth and response time of voluntary human motion. Joint velocities are calculated with period measurements in hardware, giving greater accuracy for low frequency velocity measurements. A diagram depicting the data flow is shown in Fig. 2.

B. Kinematics

A global frame of reference is set at the kinematic center of the device, where the yaw pitch and extension axes intersect; this point is the origin of Cartesian space where the x y and z axes align, as depicted in Figure 1. First the generalized coordinates for the device are set, $\vec{q} = [\theta(t)\ \phi(t)\ r(t)]^T$, where θ is the yaw, ϕ is the pitch, and r is the extension of the prismatic joint measured to the handle's grip. For the BAM the transformation into Cartesian coordinates is given by (1).

$$\vec{X} = \begin{bmatrix} r\cos(\phi)\sin(\theta) \\ r\sin(\phi) \\ r\cos(\phi)\cos(\theta) \end{bmatrix} \quad (1)$$

An Eulerian attitude matrix, A, is constructed for the purpose of transforming a vector given in a coordinate system rotated relative to the global frame into the latter. In operation the user's input forces are orthogonal to the orientation of the prismatic joint, therefore they must be transformed into the global frame using the attitude matrix A. Applying the Jacobian, $J = \frac{d\vec{X}}{d\vec{q}}$, we can determine the resulting joint torques,

$$\boldsymbol{\tau}_u = J^T A \boldsymbol{f}_u \quad (2)$$

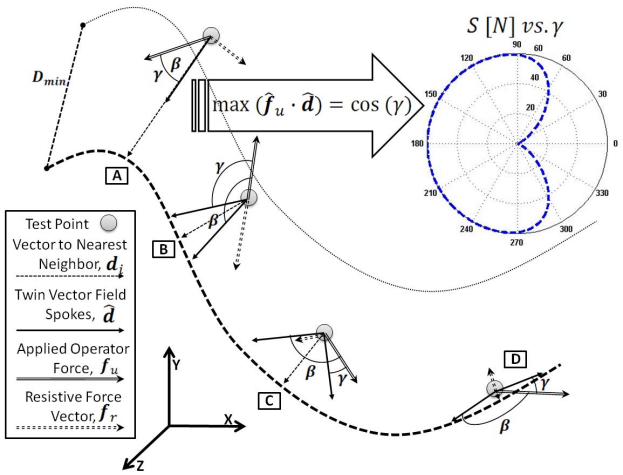

Fig 3. Diagram depicting a friction disk (top right) and several snapshots of the twinned field spokes as the user converges to the path . A) The user has not crossed into the vicinity of the linear blend. B) The vector field has split and the smallest steering angle is found. C) A component of the resistive force violates the passivity constraint. D) Twinned field spokes are almost completely tangent to the path.

III. Path Definition

A. Vector Field & Path Creation

Common approaches to path guidance require generating a timed trajectory and a controller to track this trajectory at any point in time [13-14]. The method presented here captures the path by defining a directional vector field, similar to [12], that guides the system to satisfy the trajectory, without superfluous timing information that can over constrain the system. A path is defined in the configuration space of the BAM by a point set $p_i \in P$, of length n with a positive increase in index corresponding to a forward traversal of the path. Paths of arbitrary length and complexity are input to the controller through a software teach mode.

Because of the discrete nature of the optical encoders any particular path will have a point density deficient for smooth generation of the vector field. Each path is pre-processed to increase the density to 1pt/mm using linear interpolation in three dimensions. Then rough features are smoothed by mirroring the path end to end several times and applying a zero phase forward-reverse digital filter. This path is the basis for defining the necessary vector field.

In generalized coordinate representation, a directional vector field $\boldsymbol{D}(q)$ defines at each configuration of the BAM a desired direction unit vector $\hat{\boldsymbol{d}}$. This directional vector locates the nearest neighbor i with a vector $\boldsymbol{d}_i$. $\boldsymbol{d}_i$ points along the shortest distance from q to p_i when $q \notin P$, and tangent to the contour when $q \in P$. The vector field is linearly blended to the tangent vector $\boldsymbol{d}_t$, defined by a minimum distance d_{min} as following:

$$\hat{\boldsymbol{d}} = \begin{cases} \boldsymbol{d}_i + \hat{\boldsymbol{d}}_t(\|\boldsymbol{d}_i\| - d_{\min}) & \|\boldsymbol{d}_i\| < d_{min} \\ \hat{\boldsymbol{d}}_i & \|\boldsymbol{d}_i\| > d_{min} \end{cases} \quad (3)$$

The vector field $\boldsymbol{D}(q)$ implicitly defines a positive direction of traversal along the path P in accordance with the defined tangent. To permit forward and backward motion along the contour a twin vector field is introduced so that there are two possible vector assignments possible at all times, but only one is chosen based on a steering angle. This twin has the same behavior except the linear blend points anti-parallel to $\boldsymbol{d}_t$, denoted $\boldsymbol{d}_t'$. The twinned vector field, path, and linear blend are illustrated for multiple $\hat{\boldsymbol{d}}$ at various stages of convergence (fig 3.). In order to determine which field to follow a steering angle γ is computed between the operators force vector and the twinned vector field's spokes $\hat{\boldsymbol{d}}$ using the dot product. The field producing the smallest value for γ is selected as the direction of traversal corresponding with the user's current intent. The desired vector $\hat{\boldsymbol{d}}$ from (3) is then replaced by,

$$\hat{\boldsymbol{d}} = \begin{cases} \boldsymbol{d}_i + \hat{\boldsymbol{d}}_t(\|\boldsymbol{d}_i\| - d_{\min}) & \gamma \Rightarrow \hat{\boldsymbol{d}}_t, \ \|\boldsymbol{d}_i\| < d_{min} \\ \boldsymbol{d}_i + \hat{\boldsymbol{d}}_t'(\|\boldsymbol{d}_i\| - d_{\min}) & \gamma \Rightarrow \hat{\boldsymbol{d}}_t', \ \|\boldsymbol{d}_i\| < d_{min} \\ \hat{\boldsymbol{d}}_i & \|\boldsymbol{d}_i\| > d_{min} \end{cases} \quad (4)$$

B. Locating the Nearest Neighbor

During path guidance, the user's limb position may not be on or near the desired path. To provide guidance toward the path, the nearest path location needs to be found. The nearest neighbor is simply the point on the path with the shortest distance to the current device configuration. This can be computed using a brute force method by sorting through P, although the cost, $O(n)$, of this procedure becomes prohibitive when dealing with large point sets. An alternative method is to use a k-dimensional tree to perform a recursive search, $O(\log(n))$, to locate the nearest neighbor. kd-trees provide an efficient data structure for organizing points in a k-dimensional space [15] and allow range searches to be done very efficiently. The kd-tree is often applied to collision detection for haptic environments [16] and here we apply this technique to our path guidance controllers.

IV. Path Guidance Controllers

We chose to compare three types of path guidance: velocity ratio, force cancelling, and force mapping controllers. The velocity ratio controller used on PTER [12] is chosen as a baseline for performance, and force controllers are investigated in light of the fact that a user's applied force gives clear indication as to their desired direction of motion and intention. These controllers are implemented and the subject's path guidance performance is compared.

A. Dissipative Velocity Ratio Controller

The proposed path guidance method in [12] demonstrates how the directional vector field $\boldsymbol{D}(q)$ may be used to define a desired tip velocity, $\dot{\boldsymbol{x}}_d$ at any configuration for a purely revolute device. Here we vary from the implementation in [12] with our control law (7), and prefer to use the homogenous tangent space for a spherical device to calculate

velocity ratios. This variation accounts for the BAM's prismatic joint. The desired velocities are thus defined,

$$\dot{\boldsymbol{q}}_{dt} = \left[J|_{r=1} \right]^{-1} \dot{\boldsymbol{x}}_d \tag{5}$$

Where we take the Jacobian inverse for a unit sphere to obtain tangent space velocities, $\dot{\boldsymbol{q}}_{dt}$. Because we wish the user to freely vary tip velocity, magnitude is hence unimportant, only the velocity direction is important. Therefore new states, $\dot{\boldsymbol{c}}$ are formed representing the ratios between desired and actual tangentential velocities $\dot{\boldsymbol{q}}_t$,

$$\dot{\boldsymbol{c}}_i = \dot{\boldsymbol{q}}_{dt,i} \Big/ \dot{\boldsymbol{q}}_{t,i} \ , \quad i = 1 \ldots 3. \tag{6}$$

The velocity ratios (6), are then normalized by their highest positive value, following [11], resulting in a non-dimensional numeral, $\boldsymbol{c}_n$. This vector of coefficients represents how much a link needs to slow down to obtain the desired velocity. Equation (6) fails if a component of $\dot{\boldsymbol{q}}_{t,i}$ is equal to zero, in this case that component of $\dot{\boldsymbol{c}}_i$ is set to a high value, which reduces influence on other links. There are cases when elements of $\boldsymbol{c}_n$ are less than zero, indicating that a link must switch directions, care must be taken to set the offending elements to zero. The control law is then formulated by,

$$\boldsymbol{u} = F_{max}(\mathbf{1} - \boldsymbol{c}_n)^T \tag{7}$$

Where $\boldsymbol{u}$ is the commanded joint torques, and F_{max} is a diagonal matrix formed form the product of the attitude matrix with a maximum tangential force for each axis. The maximum force is uniform across axes in the tangent space and chosen to be 30N. With the control law given in (7) the command torques will vary linearly from no actuation, when the normalized ratio is one, to the maximum set torque when the ratio is zero; essentially driving $\boldsymbol{c}_n$ to be populated by ones.

B. Force Controllers

The directional vector field $\boldsymbol{D}(q)$ can also be used as a high level force controller, with a separate low level controller computing actuator commands. The user's force information is a good indicator of directional intent and can be compared to a desired force direction, $\hat{\boldsymbol{f}}_{\boldsymbol{d}} = \widehat{\boldsymbol{d}}_d$. Two low level controllers are presented a force mapping (FM) controller, and a force cancelling (FC) controller.

1) Force Cancelling (FC) Controller

The FC controller resists any component of the user's force perpendicular to $\hat{\boldsymbol{f}}_{\boldsymbol{d}}$ with a force $\boldsymbol{f}_r$. When the user's force direction is anti-parallel $\boldsymbol{f}_r$ will vanish, because we wish to impede motion away from the path as well we define $\boldsymbol{f}_r$in this way,

$$\boldsymbol{f}_r = \begin{cases} A\boldsymbol{f}_u - \left(A\boldsymbol{f}_u \cdot \hat{\boldsymbol{f}}_{\boldsymbol{d}}\right)\hat{\boldsymbol{f}}_{\boldsymbol{d}} & A\boldsymbol{f}_u \cdot \hat{\boldsymbol{f}}_{\boldsymbol{d}} \geq 0 \\ A\boldsymbol{f}_u & A\boldsymbol{f}_u \cdot \hat{\boldsymbol{f}}_{\boldsymbol{d}} < 0 \end{cases} \tag{8}$$

The condition represented by (8) is illustrated in fig 3.b. where $\boldsymbol{f}_r$ switches modes to directly resist the user's force. Another restriction placed on $\boldsymbol{f}_r$ occurs from the passivity constraint imposed by the brakes. Energy can never be supplied to the joints thus a command torque satisfying $\tau_{r,i}\dot{q}_i > 0$ cannot be achieved (fig. 3.c). Any command violating passivity indicates that the user is already producing a desired motion along that axis, thus the actuator command is set to zero if in violation.

2) Force Mapping (FM) Controller

The FM controller uses the notion of a friction disk to define the level of friction along $\hat{\boldsymbol{f}}_r$ using the steering angle γ from (4). The friction disk is oriented on a plane containing $\hat{\boldsymbol{f}}_{\boldsymbol{d}}$ and $\boldsymbol{f}_u$, and defines a stiction level $S(\gamma)$ in such a way as to reach maximal values when $\frac{\pi}{2} < \gamma < \frac{3\pi}{2}$, and produce limited friction within an arc around $\hat{\boldsymbol{f}}_{\boldsymbol{d}}$ (fig. 3, top right). From instant to instant the disk implicitly defines a conical volume where motion is easily permitted. The mapping is based on a modified normal distribution with $\cos(\gamma)$as the pseudo random variable,

$$\sigma = -2^{\upsilon} / \ln\left(\frac{\delta}{S_{max}}\right) \tag{9}$$

$$S(\gamma) = (S_{max} + \delta) \exp\left(\frac{-(\cos(\gamma)+1)^{\upsilon}}{\sigma}\right) - \delta \tag{10}$$

Where S_{max} is the maximal system stiction to be simulated (60N), and σ is a type of variance controlled by the parameters δ & υ. The size of the diminished friction arc around $\hat{\boldsymbol{f}}_{\boldsymbol{d}}$ is controlled by varying δ. The rate of stiction increase, $dS/d\gamma$ is controlled with υ, where υ is a positive even value. The values of δ & υ are chosen to be 2 and 8 respectively, based on experimentation. The actuator commands, subject to the passivity constraint, are then generated by, $\boldsymbol{u} = J^T(S(\gamma)\hat{\boldsymbol{f}}_r)$.

V. Experimentation

A. Methods

An experiment was performed on three subjects to test the performance of each controller from section IV. The procedure entailed path guidance trials on two different paths: a simple circular loop oriented in the x-y plane, and a complex path designed to incur motion along all three kinematic axes. Each subject was given a time limit for path traversal of either 10 or 20 seconds for the circular and complex path respectively. Initially a subject traverses the path without a controller present to obtain a ground truth estimate. Then trials were performed using the three different control techniques.

In order to test controller proficiency further we tested with and without visual feedback. In total each subject performed 16 (2 paths, 4 conditions, with/without visualization) trials where position, joint torque, nearest

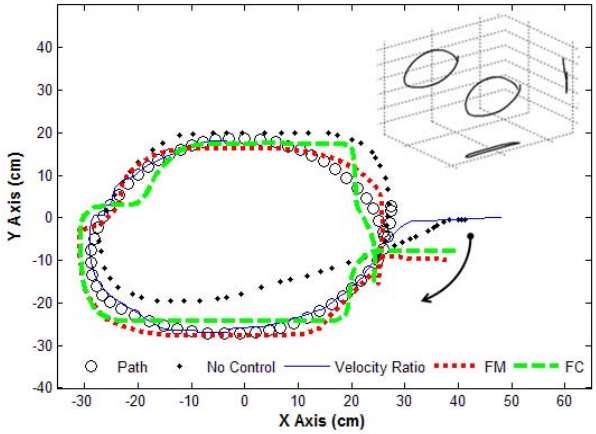

Fig 4. An X-Y projection of the circular path, showing subject A's motions for each control technique. The direction of traversal is indicated, and an isometric view of the path is inset at upper right.

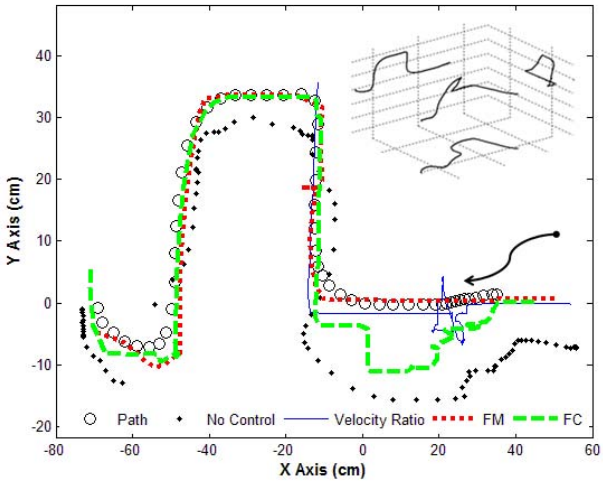

Fig 5. An X-Y projection of the complex path, showing subject A's motions for each control technique. The direction of traversal is indicated, and an isometric view of the path is inset at upper right.

neighbor, and time were recorded. The trials without visual feedback were conducted upon completion of the visual feedback section.

B. Results

Figures 4 & 5 illustrate the typical user motions for simple and complex paths in a visual feedback regime. Figure 6 shows the cumulative error which is an integral of guidance error, $\|\boldsymbol{d}_i\|$. In the no control and velocity control model, the subjects were often unable to traverse the entire path in the allotted time. To augment this result, the x-axis represents the percent of path traversed. This parametric plot helps show if a user has stalled, indicating trouble points at the particular percentage of path traversal. Figure 7 shows the torque profiles under different controllers to highlight the chatter shown for the velocity ratio controller.

The data shows trial motions with velocity ratio control failed to traverse more than 50% of the path 75% of the time. In contrast the force controllers allowed movement along 90% of the path 75% of the time. The 25% failure rate for the force controllers is wholly due to trials without visual feedback on the complex path. The average guidance errors, with standard deviations, across all cases can be found at the

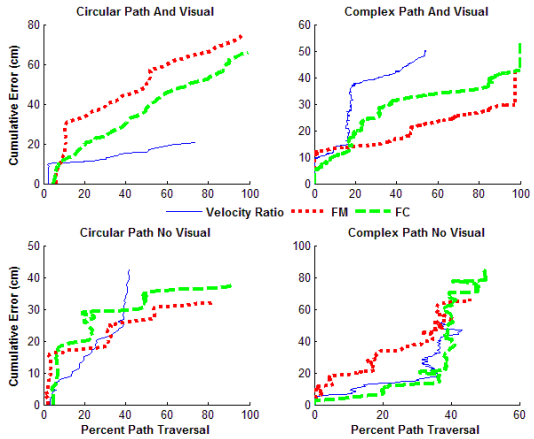

Fig 6. Subject A's error plots depicting performance of all three control techniques. Top plots show the case of visual feedback, and left plots show the circular path.

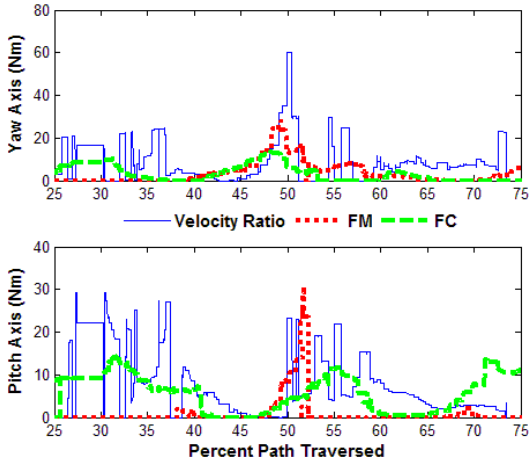

Fig 7.Individual joint torques from a single subject's trial, using visual feedback on the circular path. Each torque is parameterized over the percent path traversed. Plots are shown for the median path section from 25-75%.

end in table 1. Overall there was no statistical difference in error magnitude between the three controller conditions. This implies the force controllers perform similarly in the error domain as velocity control.

For all controllers on the circular path, lack of visual feedback significantly increased error ($p<0.03$). While error still increased on the complex path without visual feedback, there was no statistical difference between controller performance ($p>0.12$). Interestingly, the average errors for force control throughout all conditions are significantly different than the ground truths ($p<0.05$), while no such claim can be made for the velocity ratio's error in the condition of no visual feedback ($p>0.22$) irrespective of path.

VI. Discussion

Most notable difference between controllers is the fact that subjects could not complete the path in an allotted time under velocity control. The cause of the velocity ratio's slow performance is believed to stem from two sources. One, the requirement for accurate low frequency velocity

measurements, and two chatter in the actuator commands. The torque profiles (fig. 7) indicate discontinuous actions from the velocity ratio controller, making it difficult to maintain a steady velocity in any direction. The torque profiles from the force controllers are noticeably smoother, producing less stop and go motion allowing greater and easier rate of travel. This was consistent with a questionnaire where each subject stated that force control was markedly smoother.

Comparing the resultant motions from the force controllers we see that the FC technique tends to produce large stepped motions (Fig. 4-5). This artifact results from the user consistently applying large average forces while testing the vector field for the correct direction. When this direction was found the user can overshoot the path before the brakes apply a correction. The FM control technique had the advantage, because it reduced the constraints imposed from direct force cancellation with the mapping $S(\gamma)$, producing overall smoother trajectories, and less overshoot.

Analyzing the cumulative error plots (Fig. 6) we can see there is a relationship between path curvature and error magnitude. The circular path, while having practically constant curvature exhibits a stair case effect on the parametric plots. These steps arise when the user's Cartesian velocity switches direction along an axis and the user is jarred to a stop by their own inertia carrying them in the wrong direction. This is the fundamental difference and trouble with "path guidance" which is exacerbated without visual feedback. This can be seen (Fig. 6) by the increase in stepped behavior with no visual cues. A similar effect is present for the complex path with noticeable areas of difficulty located around 20 and 40 percent path traversal. At these points the path makes acute turns into different Cartesian planes. In particular the transition across the 40% mark is very difficult without visual feedback.

Our results indicate that visual feedback is an important factor for successful controller on a dissipative haptic device. This was especially true when the visual feedback provided clearer information such as the circular path. For the complex path, the visual feedback itself was difficult to interpret because it was presented on a 2D computer screen. This issue is specifically related to the difference between path following and path guidance; a passive device must rely on some system of outward intent, separate from the controller, to energize the system and eventually minimize error. This intent comes from a user's visual feedback allowing a context to be placed around a path in 3D space. Any device that reduces the subject's kinesthetic awareness and heightens their visual acuity will help co-locate haptic objects in the body space and could be used to enhance the path guiding performance of a dissipative haptic device.

To help path guidance further more context needs to be supplied visually to provide correct 3D perception. We will use a wearable system with a head tracker, providing more surrounding information to enhance this effect.

The force controllers presented here allowed smooth control laws that may be suitable for rehabilitation with a dissipative device. Incorporating energy storage elements into the BAM, and manipulating psychophysical relations between the subject and a virtual environment, through visual distortion, may lead the way to providing true path following for purely dissipative devices.

TABLE I
Average Error Comparison for All Subjects

	With Vis. Feedback		Without Vis. Feedback	
Circular	Error [cm]	Std. Dev.	Error [cm]	Std. Dev
No Control	12.8	5.44	17.9	6.72
Vel. Ratio	4.62	1.72	11.5	3.57
FM	3.22	0.26	7.18	1.70
FC	3.26	0.81	6.01	1.58
Complex	Error [cm]	Std. Dev.	Error [cm]	Std. Dev
No Control	10.4	2.40	14.4	4.22
Vel. Ratio	4.98	1.82	10.7	2.89
FM	4.10	0.96	6.34	1.13
FC	5.22	1.30	6.74	1.27

VII. REFERENCES

[1] J. Patton, Y. Wei, C. Scharver, R.V. Kenyon, R. Scheidt, "Motivating Rehabilitation by Distorting Reality," Inter. Conf. on Biomedical Robotics and Biomechatronics, pp. 869-874, 2006.

[2] B.R. Brewer, M. Fagan, R. Klatzky, Y. Matsuoka, "Perceptual Limits for a Robotic Rehabilitation Environment Using Visual Distortion," IEEE Trans. On Neural Systems and Rehabilitation Engineering, Vol. 13, pp. 1-11, 2005.

[3] H.I. Krebs, N. Hogan, M.L. Aisen, B.T. Volpe, "Robot Aided Neurorehabilitation," IEEE Transactions on Rehabilitation Engineering, pp. 75-87, 1998.

[4] P.S. Lum, C.G. Burgar, P.C. Shor, M. Majmundar, M. Van der Loos, "Robot-assisted movement training compared with conventional therapy techniques for the rehabilitation of upper-limb motor function after stroke," Arch. phys. med. Rehabilitation, Vol. 83, pp.952-959, 2002.

[5] M. Zinn, O. Khatib, B. Roth, J.K. Salisbury, "Playing it safe [human-friendly robots]," Robotics & Automation Mag., Vol. 11(2), pp. 12-21, 2004.

[6]F. Conti, O. Khatib, C. Baur, "A Hybrid Actuation Approach for Haptic Devices," Proc. of Symp. On Haptic Interfaces for Virtual Environment and Teleoperator Systems, pp. 367-372, 2007.

[7] J. E. Colgate, W. Wannasuphoprasit, M.A. Peshkin, "Cobots: Robots for collaboration with human operators," IMECE, 1996.

[8] M.V. Weghe, B. Dellon, S. Kelly, R. Juchniewicz, Y. Matsuoka, "Demonstration of a Large Dissipative Haptic Environment," IEEE Virtual Reality Conf. pp. 49, 2006.

[9] C. Cho, M. Kim, J.B. Song, "Direct Control of a Passive Haptic Device Based on Passive Force Manipulability Ellipsoid Analysis," Int. Journal of Control, Automation, and Systems, Vol. 2(2), pp. 238-246, 2004.

[10] Y. Matsuoka, W. T. Townsend, "Design of lifesize haptic environments", Experimental Robotics VII, Rus and Singh, ed, 2001.

[11] D.K. Swanson, W.J. Book, "Obstacle Avoidance Methods for a Passive Haptic Display," IEEE Int. Conf. on Advanced Intelligent Mechatronics,Vol. 2, pp. 1187-1192, 2001.

[12] D.K. Swanson, W.J. Book, "Path-following control for dissipative passive haptic displays," Proc. Haptic Interfaces for Virtual Environment and Teleoperator Systems, pp. 101-108, 2003.

[13] O. Khatib, "Unified Approach for Motion and Force Control of Robot Manipulators: the Operational Space Formulation." IEEE Journal of Robotics and Automation, Vol. 3(1), pp. 43-53, 1987.

[14] D. Feygin, M. Keehner, R. Tendick, "Haptic guidance: experimental evaluation of a haptic trainingmethod for a perceptual motor skill," Proc. Haptic Interfaces for Virtual Environments and Teleoperator Systems, pp. 40-47, 2002.

[15] Z.L. Cai, J. Dill, S. Payandeh, , "Haptic rendering: practical modeling and collision detection" Proc. ASME Virtual Environment and Teleoperator System Symp. Vol. 67, pp. 81-86. 1999.

[16] J. L. Bentley, "Multidimensional Binary Search Trees Used for Associative Searching," Commun. ACM, Vol. 18(9), pp. 509-517, 1975.